ACS APPLIED NANO MATERIALS

www.acsanm.org Article

CD7 Nanobody-Based Immuno-Nanotoxin for Targeted Treatment of T-Cell Acute Lymphoblastic Leukemia

Yangyang Dong, Fengtao You, Yifan Zhang, Huanli Sun,* Ru Cheng, Songsong Zhao, Lin Yang,* and Zhiyuan Zhong*

Cite This: *ACS Appl. Nano Mater.* 2024, 7, 7195−7202 Read Online

ACCESS | Metrics & More | Article Recommendations | Supporting Information

ABSTRACT: T-cell acute lymphoblastic leukemia (T-ALL) has been plagued by high relapse and mortality rates due to the lack of available targeted treatment options in the clinic. Herein, a CD7-specific immuno-nanotoxin based on anti-CD7 nanobody-modified polymersome-mertansine nanoconjugates (aCD7-Ps-DM1) was engineered to enable effective and targeted chemotherapy of orthotopic T-ALL in vivo. aCD7-Ps-DM1 with regulable aCD7 density showed no DM1 leakage while rapid DM1 release under reducing conditions. The aCD7-Ps-DM1 immuno-nanotoxin efficiently targeted CD7-positive CCRF-CEM T-ALL cells, leading to 5-fold and >13-fold greater anti-ALL activity than that of nontargeted Ps-DM1 and CD7-negative B-ALL cell lines, respectively. In orthotopic CCRF-CEM T-ALL-bearing mice, repetitive (multiple) dosing of aCD7-Ps-DM1 persistently inhibited leukemia progression and infiltration in the bone marrow, blood, and organs, leading to significantly improved survival. This CD7-specific immuno-nanotoxin may offer a potential targeted treatment strategy for T-ALL.

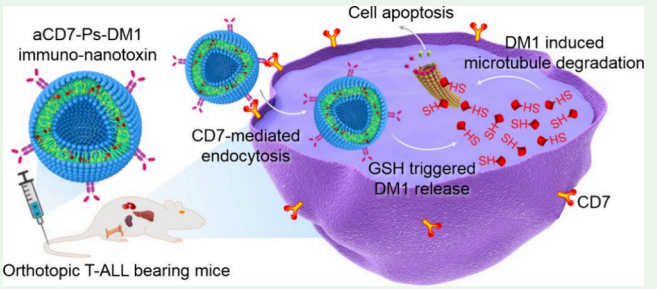

KEYWORDS: *leukemia, targeted therapy, mertansine, polymersomes, drug conjugates*

1. INTRODUCTION

T-cell acute lymphoblastic leukemia (T-ALL) is a highly aggressive and heterogeneous hematological malignancy of T-cell progenitors that is associated with a high relapse rate and mortality.[1,2] Intensive chemotherapy, as the standard and first-line treatment, has substantially improved the survival outcomes of T-ALL patients who can tolerate it.[3−5] However, the clinical prognosis of frail patients intolerant to chemotherapeutics and relapsed patients resistant to chemotherapy remains poor as a result of the severe lack of therapeutic options.[6−8] Nelarabine, the only drug approved for treating relapsed and refractory T-ALL patients, only achieved a one-year overall survival of ca. 24% and carried a boxed warning for severe neurotoxicity.[9−12] Therefore, there is a desperate need to develop effective and safe therapeutic options.

Unlike B-cell ALL, which has well-validated targets (CD19, CD20, and CD22) and a variety of FDA-approved immunotherapies, including monoclonal antibodies, bispecific antibodies, antibody-drug conjugates (ADCs), and chimeric antigen receptor (CAR)-T cells, the lack of mature and specific targets of T-ALL is a major reason underlying its dismal clinical prognosis.[13−16] CD7, a T-lineage-specific antigen, is overexpressed in T-ALL and known to mediate endocytosis, making it an attractive target for treating T-ALL recently.[17−19] Several CD7 CAR-T cell therapies are under early clinical evaluation and have shown some response.[20−23] However, the development of CD7 CAR-T cells is complicated, costly, and associated with major challenges, such as cytokine release syndrome and fratricide.[24,25]

Herein, a CD7-specific immuno-nanotoxin was engineered by clicking anti-CD7 nanobody onto the surface of polymersome-mertansine nanoconjugates (aCD7-Ps-DM1) for targeted chemotherapy of T-ALL in vivo (Scheme 1). DM1, a common warhead for ADCs, has been reported to inhibit microtubule depolymerization and has high potency against both solid and hematological tumors.[26−28] The aCD7-Ps-DM1 immuno-nanotoxin with disulfide-linked DM1, reversible membrane cross-linking, and tunable aCD7 density was constructed via the assembly of dithiolane rings containing amphiphilic copolymers and a post-click reaction, which showed zero DM1 leakage but fast DM1 release under reductive conditions. Intriguingly, the aCD7-Ps-DM1 immuno-nanotoxin induced 5-fold greater anti-T-ALL activity than the Ps-DM1 nanotoxin in CD7-positive CCRF-CEM cells and potently reduced the

Received: December 28, 2023
Revised: March 6, 2024
Accepted: March 8, 2024
Published: March 21, 2024

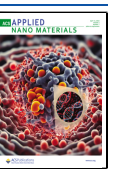

Scheme 1. Construction of a CD7-Specific Immuno-Nanotoxin Based on Anti-CD7 Nanobody-Modified Polymersome-DM1 Nanoconjugates (aCD7-Ps-DM1) for Targeted Chemotherapy in an Orthotopic T-ALL Model

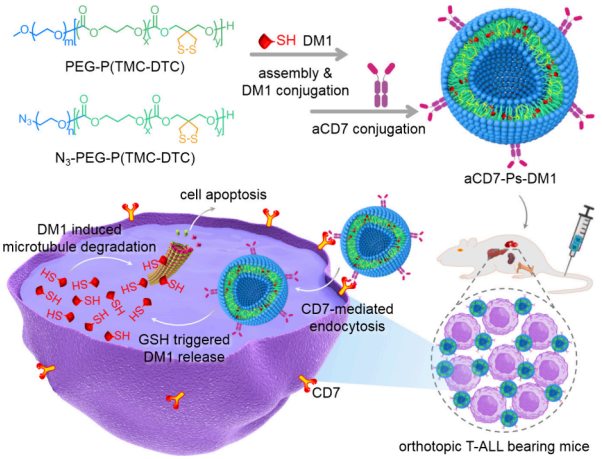

leukemia burden in orthotopic CCRF-CEM T-ALL bearing mice, providing a significant survival benefit.

2. EXPERIMENTAL SECTION

2.1. Materials. An anti-CD7 nanobody (aCD7) with the same sequence as described in a previous report[29] was provided by PersonGen BioTherapeutics (Suzhou) Co., Ltd. NHS-PEG$_4$-DBCO (97%) was obtained from BroadPharm. Mertansine (DM1) was purchased from Brightgene Bio-Medical Technology Co., Ltd. Glutathione (GSH, 99%) was purchased from J&K Scientific. Dithiothreitol (DTT, >99%) and 4′,6-diamidino-2-phenylindole (DAPI) were obtained from Beyotime Biotechnology. Cell Counting Kit-8 (CCK8) was obtained from Suzhou Fcmacs Biotech Co., Ltd. 3-(4,5-dimethylthiazol-2-yl)-2,5-diphenyltetrazolium bromide (MTT) was obtained from Solarbio Life Science. An Annexin V-APC/7-AAD apoptosis kit was obtained from MultiSciences. Cyanine 5-NH$_2$ (Cy5) was obtained from Beijing Fanbo Biochemicals Co., Ltd. Anhydrous ethanol, *N*,*N*′-dimethyl formamide (DMF), and dimethyl sulfoxide (DMSO) were purchased from Sinopharm Chemical Reagent Co., Ltd. All of the reagents were used as received. Poly(ethylene glycol)-*b*-poly(trimethylene carbonate-*co*-dithiolane trimethylene carbonate) (PEG-P(TMC-DTC), $\bar{M}_n$ = 5.0 − (15.1−2.0) kg/mol, $\bar{M}_w/\bar{M}_n$ = 1.1) and N$_3$-PEG-P(TMC-DTC) ($\bar{M}_n$ = 7.9 − (15.1−2.0) kg/mol, $\bar{M}_w/\bar{M}_n$ = 1.1) copolymers were synthesized similarly to our previous reports.[30−32]

2.2. Preparation of Azide-Functionalized Polymersome-DM1 Nanoconjugates (N$_3$-Ps-DM1). N$_3$-Ps-DM1 was prepared via coassembly of PEG-P(TMC-DTC) and N$_3$-PEG-P(TMC-DTC) (98:2 in weight) with concurrent DM1 conjugation via thiol−disulfide exchange reactions of the thiol group of DM1 with dithiolane rings in the vesicular membrane. In brief, 22.5 mL of phosphate buffer (PB, 10 mM, pH 7.4) was mixed with 1 mL of DM1 solution in DMF (10 mg/mL) under stirring at 180 rpm and 37 °C, followed by injection of 2.5 mL of polymer solution in DMF (40 mg/mL). After overnight incubation at 37 °C and 100 rpm, the suspension was dialyzed (MWCO: 14 kDa) sequentially against PB (10 mM, pH 7.4) for 4 h, PB containing 20% ethanol for 48 h, and PB to obtain N$_3$-Ps-DM1. The size and size distribution of N$_3$-Ps-DM1 were measured by dynamic light scattering (DLS). To verify that DM1 was covalently conjugated rather than physically loaded in the polymersomes, 100 μL of N$_3$-Ps-DM1 was mixed with 900 μL of acetonitrile and incubated overnight at 37 °C for high-performance liquid chromatography (HPLC) analysis. To determine the amount of DM1 inside N$_3$-Ps-DM1, 100 μL of N$_3$-Ps-DM1 was incubated overnight with 900 μL of DTT solution in acetonitrile (20 mM DTT) at 200 rpm and 37 °C. Then, it was measured by HPLC at 252 nm using acetonitrile and water (v/v = 60/40) as the mobile phase. The DM1 content was calculated according to the DM1 standard curve, thus calculating the DM1 conjugation content by comparing the weight of conjugated DM1 to the total weight of polymers and conjugated DM1.

Similarly, Cy5-labeled polymersomes (N$_3$-Ps-Cy5) were fabricated via coassembly of N$_3$-PEG-P(TMC-DTC), PEG-P(TMC-DTC)-Cy5, and PEG-P(TMC-DTC) at a weight ratio of 2:4:94.

2.3. Preparation of Anti-CD7 Nanobody-Engineered Polymersome-DM1 Nanoconjugates (aCD7-Ps-DM1). aCD7-Ps-DM1 was obtained via a copper-free click reaction of N$_3$-Ps-DM1 with dibenzocyclooctyne-functionalized anti-CD7 nanobody (aCD7-DBCO), which was synthesized by reacting aCD7 with NHS-OEG$_4$-DBCO. To prepare aCD7-DBCO, 1.5 mL of aCD7 solution (2 mg/mL, ∼80,000 g/mol) was mixed with 14.6 μL of NHS-OEG$_4$-DBCO (5 mg/mL in DMSO, 649.7 g/mol) at a molar ratio of 1:3 and reacted at 4 °C for 12 h, followed by ultrafiltration (MWCO: 10 kDa) to remove the unreacted NHS-OEG$_4$-DBCO. The concentration of aCD7-DBCO was determined by HPLC with a mobile phase of PBS (150 mM NaCl, 50 mM PB, pH 6.8):acetonitrile = 9:1, detection wavelength of 214 nm, and column temperature of 30 °C. The degree of DBCO functionalization was analyzed by matrix-assisted laser desorption/ionization time-of-flight mass spectrometry (MALDI-TOF-MS).

aCD7-Ps-DM1 with different aCD7 densities was then prepared via click reaction of N$_3$-Ps-DM1 with aCD7-DBCO at different aCD7-to-N$_3$ molar ratios (0.25:1, 0.5:1, and 1:1). Taking 0.5:1 as an example, 158 μL of aCD7-DBCO (0.77 mg/mL) was added to 188 μL of N$_3$-Ps-DM1 (20 mg/mL in PB) for an overnight reaction at 4 °C. Then, aCD7-Ps-DM1 was acquired by three rounds of ultrafiltration (MWCO: 300 kDa) against PBS, after which the ultrafiltrate was collected to quantify the unreacted aCD7-DBCO by HPLC and therefore the amount of aCD7 conjugated to Ps-DM1. The number of aCD7 molecules per Ps was calculated according to the following equation, wherein the molecular weight (MW) of each polymersome (M_w: 1.54 × 10^7 g/mol) was reported in our previous work.[33]

$$\text{Number of a CD7 per Ps} = \frac{\text{mass of conjugated a CD7}}{\text{MW of a CD7}} \times \frac{\text{MW of each polymersome}}{\text{mass of polymersomes}}$$

The size, size distribution, and stability of aCD7-Ps-DM1 were detected by DLS. To confirm the release of native DM1 under reducing conditions, aCD7-Ps-DM1 was incubated at 37 °C for 24 h either with or without 10 mM GSH and measured by HPLC, using free DM1 as a control.

In vitro drug release from aCD7-Ps-DM1 was carried out in two different media, PB (10 mM, pH 7.4) and PB with 10 mM DTT. In brief, 0.5 mL of aCD7-Ps-DM1 (0.5 mg/mL) was dialyzed (MWCO: 14 kDa) against 25 mL of the release media at 37 °C and 200 rpm. At 2, 4, 6, 8, 12, and 24 h, 5 mL of release media was taken out and replaced with the same volume of fresh media. The DM1 concentration in the release media was determined via HPLC to calculate the cumulative DM1 release. The final values are displayed as the mean ± standard deviation (SD) (n = 3).

2.4. Cellular Uptake Studies. The targetability and cellular uptake of aCD7-Ps-DM1 in CD7-positive CCRF-CEM cells were studied via flow cytometry and confocal laser scanning microscopy (CLSM) utilizing Cy5-labeled polymersomes (aCD7-Ps-Cy5 and Ps-Cy5). CD7-negative 697 ALL cells were used as a control. For flow cytometry analysis, CCRF-CEM or 697 cells seeded in six-well plates (2 × 10^5 cells/well) were incubated with 100 μL of aCD7-Ps-Cy5 at different aCD7 surface densities or Ps-Cy5 (Cy5: 2.0 μg/mL). After 4 h of incubation, the cells were centrifuged at 800 rpm for 5 min, washed twice with PBS, and finally dispersed in 500 μL of PBS for measurements.

For CLSM studies, sterilized cell slides in a 24-well plate were incubated overnight with polylysine (800 μL, 0.1 mg/mL). After thorough washing with PBS, CCRF-CEM cells were seeded into the plate (3 × 10^5 cells/well) for 4 h, after which 200 μL of aCD7-Ps-Cy5, Ps-Cy5, or PBS was added to each well (Cy5: 20 μg/mL) for

https://doi.org/10.1021/acsanm.3c06253
ACS Appl. Nano Mater. 2024, 7, 7195−7202

another 4 h of incubation. Then, the cells were gently washed with PBS 3 times, fixed with 4% paraformaldehyde (500 μL) for 15 min, and stained with DAPI for 3 min. After each step, the cells were washed 3 times with PBS. Finally, cell slides with adherent cells were mounted onto microscope slides using glycerol to take CLSM images.

2.5. In Vitro Anti-ALL Activity of aCD7-Ps-DM1 Immuno-Nanotoxin. The in vitro anti-ALL effects of aCD7-Ps-DM1 in CD7-positive CCRF-CEM T-ALL cells as well as in CD7-negative Nalm-6-Luc and 697 B-ALL cells were determined by the CCK8 assay. Nontargeted Ps-DM1 and free DM1 served as the controls. A total of 80 μL of cell suspension was added to each well of 96-well plates (1.5×10^4 cells/well) and incubated in a cell incubator at 37 °C and 5% CO_2. Then, 20 μL of aCD7-Ps-DM1 bearing different aCD7 densities, Ps-DM1, and free DM1 in PBS were added to each well at DM1 concentrations of 0.0004, 0.004, 0.04, 0.4, 10, 40, and 100 ng/mL, respectively. Cells cultured with 20 μL of PBS were used as a control. After 48 h of incubation, 10 μL of the CCK8 solution was added to each well for an additional 4 h of incubation, after which the absorbance at 450 nm was determined via a microplate reader. Cell viability was calculated by comparing the absorbance to that of PBS-treated control cells.

The cytotoxicity of aCD7-Ps-DM1 toward normal cells, including human T cells and mouse L929 fibroblasts, was also studied. T cells in 96-well plates (4×10^4 cells/well) were incubated with aCD7-Ps-DM1 at DM1 concentrations of 2−100 ng/mL for 48 h, followed by an additional 4 h of incubation with CCK8 and absorbance measurement at 450 nm. L929 fibroblasts were seeded in 96-well plates (4000 cells/well) and cultured for 12 h. Then, 20 μL of aCD7-Ps-DM1 in PBS was added to yield final DM1 concentrations of 10, 40, 100, 200, and 1000 ng/mL. Cells cultured with only PBS served as a control. After 48 h of incubation, 10 μL of the MTT solution in PBS (5 mg/mL) was added, followed by another 4 h of culture. The medium was carefully removed, and 150 μL of DMSO was added to each well to dissolve the resulting purple formazan. The absorbance of each well at 570 nm was detected by a microplate reader to calculate the cell viability. The cytotoxicity of the free aCD7 nanobody toward CCRF-CEM cells was studied via the CCK8 assay, as described above. The aCD7 concentration ranged from 2 to 1000 ng/mL.

2.6. Proapoptotic Effect of aCD7-Ps-DM1. The proapoptotic effects of aCD7-Ps-DM1 and Ps-DM1 on CCRF-CEM cells were determined by flow cytometry using an Annexin V-APC/7-AAD apoptosis kit. CCRF-CEM cells in 6-well plates (1×10^6 cells/well) were incubated with 200 μL of aCD7-Ps-DM1 or Ps-DM1 at a DM1 concentration of 1 ng/mL for 4, 12, or 24 h. In the control group, the cells were incubated with 200 μL of PBS similarly. After centrifugation and washing with cold PBS, 500 μL of 1× binding buffer was added to resuspend the cells. Then, 5 μL of Annexin V-APC and 10 μL of 7-AAD were added for 5 min of staining prior to flow cytometry analysis. Cells treated with the positive control solution according to the protocol were stained with either Annexin V-APC or 7-AAD and used as single-positive controls.

2.7. In Vivo Anti-T-ALL Effect. All animal procedures were performed under protocols approved by the Soochow University Laboratory Animal Center and the Animal Care and Use Committee of Soochow University. The in vivo anti-T-ALL activity of aCD7-Ps-DM1 was evaluated in a disseminated CCRF-CEM T-ALL model, which was established via tail vein injection of 5×10^5 CCRF-CEM cells into each female B-NDG mouse (6−8 weeks, Biocytogen) on day 0. Five days after T-ALL inoculation, orthotopic CCRF-CEM T-ALL-bearing mice were randomly divided into three groups of 9 mice each and intravenously injected with aCD7-Ps-DM1, Ps-DM1, or PBS. The DM1 dosage was set at 0.2 mg/kg, and 5 injections were administered in total for each group at an interval of 4 days. In each group, 4 mice were used to detect the T-ALL burden in different organs, and another 5 mice were used to monitor the body weight change, T-ALL burden in the peripheral blood and survival. The mice were weighed every 2 days. On days 21, 24, and 26/27, peripheral blood was collected to monitor T-ALL progression. On day 26, 4 mice in each group were sacrificed, and the spleen, liver, and bone marrow were collected to determine the T-ALL burden. In brief, the collected samples were ground into single cells, lysed with 5 mL of ACK red blood cell lysate (1 L ACK: 8.29 g of NH_4Cl, 1 g of $KHCO_3$, and 37.2 mg of Na_2EDTA, pH 7.2−7.4), and stained with an APC-conjugated antihuman CD45 antibody (APC-hCD45, Biolegend) for flow cytometry analysis. Major organs and hind limbs were also fixed with 4% paraformaldehyde, sliced, and stained with hematoxylin and eosin (H&E) for histological analysis.

Subsequently, the anti-T-ALL activity of aCD7-Ps-DM1 was further studied after the intensive administration. On day 3 post-T-ALL inoculation, orthotopic CCRF-CEM T-ALL-bearing mice were randomly grouped ($n = 5$) and treated with PBS, Ps-DM1, or aCD7-Ps-DM1 (0.2 mg DM1 equiv./kg). A total of 8 injections were given at an interval of 4 days. The weight and survival of the mice were continuously monitored. The T-ALL burden in the peripheral blood was monitored on day 26 for all of the groups and on day 34 for the aCD7-Ps-DM1-treated group.

2.8. Statistical Analysis. The data are presented as the mean ± SD. Significant differences between different groups were analyzed by one-way ANOVA with Tukey's post hoc test. Kaplan−Meier survival curves were compared by the log-rank test. $^*p < 0.05$, $^{**}p < 0.01$, and $^{***}p < 0.001$.

3. RESULTS AND DISCUSSION

3.1. Fabrication and Characterization of aCD7-Ps-DM1 Immuno-Nanotoxin. DM1 is a microtubule-interfering agent with potent and broad-spectrum antitumor activity but cannot be used alone due to its strong systemic toxicity.[34−36] Nanomedicines are believed to improve the pharmacokinetics and reduce the side effects of chemotherapeutics,[37,38] which may expand the clinical application of DM1. In particular, targeted delivery nanosystems that can stably load DM1 to prevent leakage and deliver it specifically to the tumor site are desired, but limited research is currently available. Herein, anti-CD7 nanobody-engineered polymersome-DM1 nanoconjugates (aCD7-Ps-DM1)-based CD7-specific immuno-nanotoxin with covalent DM1 conjugation and reduction-triggered DM1 release was designed for targeted treatment of T-ALL, for which effective targeted strategies are lacking.

aCD7-Ps-DM1 was facilely engineered by clicking aCD7-DBCO on the surface of N_3-Ps-DM1. N_3-Ps-DM1 was prepared from the coassembly of N_3-PEG-P(TMC-DTC) and PEG-P(TMC-DTC) (2:98 in weight) with concurrent disulfide cross-linking and DM1 conjugation, similar to our previous reports,[33,39] which showed a size of 44 nm, a PDI of 0.16 (Figure S1) and a DM1 conjugation content of 5.4 wt %. aCD7-DBCO with an average of two DBCO groups on each nanobody was synthesized via an amidation reaction of the anti-CD7 nanobody with 3 mol equiv of NHS-OEG_4-DBCO (Figure 1a). Upon adjusting the molar feed ratio of aCD7-DBCO to N_3 on the surface of N_3-Ps-DM1 from 0.25:1, 0.5:1 to 1:1, $aCD7_x$-Ps-DM1 with 1.5, 5.2, and 8.5 aCD7 molecules per Ps-DM1 was conveniently fabricated (Table 1). The resulting $aCD7_x$-Ps-DM1 exhibited a slightly larger size (48−50 nm) than did N_3-Ps-DM1, a narrow PDI (0.16−0.21) and high stability against 50-fold dilution (Figure 1b,c and Table 1). As a result of covalent DM1 conjugation via disulfide linkages, $aCD7_{5.2}$-Ps-DM1 was quite stable in PB with no DM1 leakage, while rapidly released native DM1 after incubation with 10 mM GSH (Figure S2). Cumulative DM1 release studies further showed that ca. 80% of DM1 was released in 12 h from $aCD7_{5.2}$-Ps-DM1 under reductive conditions with 10 mM DTT (Figure 1d).

3.2. Cellular Uptake and In Vitro Anti-T-ALL Effect of aCD7-Ps-DM1 Immuno-Nanotoxin. CD7 is highly expressed in T-ALL and has recently become a popular target

https://doi.org/10.1021/acsanm.3c06253
ACS Appl. Nano Mater. 2024, 7, 7195−7202

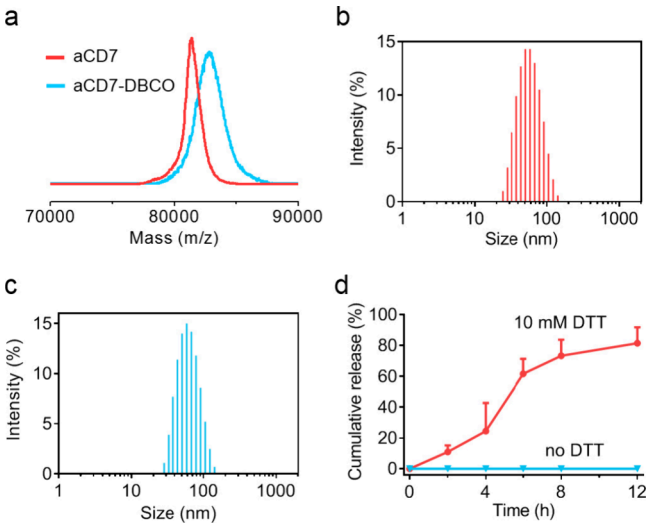

Figure 1. (a) MALDI-TOF-MS spectra of aCD7 and aCD7-DBCO. Size distributions of (b) $aCD7_{5.2}$-Ps-DM1 and (c) that after 50-fold dilution. (d) In vitro DM1 release from $aCD7_{5.2}$-Ps-DM1 in PB and PB containing 10 mM DTT (n = 3).

Table 1. Characterization of aCD7-Ps-DM1 with Diverse aCD7 Nanobody Densities

polymersomes	feeding molar ratio aCD7-DBCO:N_3	aCD7 density (number per Ps)[a]	size (nm)[b]	PDI[b]
N_3-Ps-DM1			44	0.16
$aCD7_{1.5}$-Ps-DM1	0.25:1	1.5	49	0.21
$aCD7_{5.2}$-Ps-DM1	0.5:1	5.2	50	0.17
$aCD7_{8.5}$-Ps-DM1	1:1	8.5	48	0.16

[a]Determined by HPLC. [b]Measured by DLS (25 °C).

for treating T-ALL, as supported by multiple clinical trials of CD7 CAR-T cells.[40−42] Herein, CD7-positive CCRF-CEM T-ALL cells were used to study the cellular uptake and anti-T-ALL effect of aCD7-Ps-DM1 using CD7-negative Nalm-6-Luc and 697 B-ALL cells as well as normal human T cells and mouse L929 cells as controls. To investigate the cellular uptake of aCD7-Ps-DM1, Cy5-labeled polymersomes, including aCD7-Ps-Cy5 with diverse aCD7 surface densities and nontargeted Ps-Cy5, were prepared. Flow cytometry analysis of CCRF-CEM T-ALL cells revealed that aCD7-Ps-Cy5 with either 1.5, 5.2, or 8.5 aCD7 on the surface had approximately 3.3-fold higher cellular uptake than Ps-Cy5 (Figure 2a). However, the cellular uptake of $aCD7_{5.2}$-Ps-Cy5 in CD7-negative 697 cells was similar to that of Ps-Cy5 (Figure S3). CLSM images further confirmed the enhanced cellular uptake of $aCD7_{5.2}$-Ps-Cy5 in CCRF-CEM T-ALL cells, as shown by the stronger intracellular Cy5 fluorescence in comparison to that in Ps-Cy5-treated cells (Figure 2b).

In line with the results of the cellular uptake studies, aCD7-Ps-DM1 immuno-nanotoxin with different targeting densities potently inhibited the proliferation of CCRF-CEM T-ALL cells (Figure 2c). $aCD7_{5.2}$-Ps-DM1, which has the highest anti-T-ALL activity, exhibited a half-maximal inhibitory concentration (IC_{50}) of 0.3 ng/mL, 63.7 and 5.0-fold lower compared to that of free DM1 (19.1 ng/mL) and Ps-DM1 (1.5 ng/mL), respectively. However, in CD7-negative 697 and Nalm-6-Luc B-ALL cells, the cytotoxicity of $aCD7_{5.2}$-Ps-DM1 was equivalent to that of Ps-DM1, showing IC_{50} values of 3.6

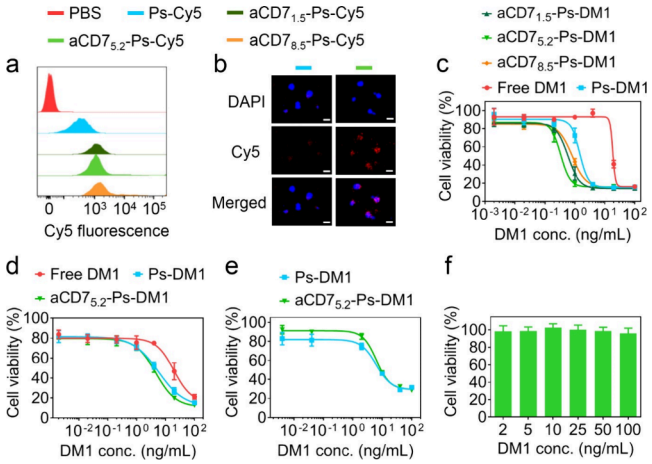

Figure 2. Cellular uptake of aCD7-Ps-Cy5 and Ps-Cy5 in (a) CD7-positive CCRF-CEM T-ALL cells. (b) CLSM images of CCRF-CEM cells following 4 h of incubation with $aCD7_{5.2}$-Ps-Cy5 or Ps-Cy5 (scale bars: 50 μm). Cytotoxicity of aCD7-Ps-DM1 in (c) CCRF-CEM, (d) 697, (e) Nalm-6-Luc, and (f) human T cells (n = 4). Ps-DM1 and/or free DM1 were used as controls.

and 9.2 ng/mL, respectively, which were 12.0−30.7-fold greater than that of $aCD7_{5.2}$-Ps-DM1 in CD7-positive CCRF-CEM cells (Figure 2d,e). More importantly, $aCD7_{5.2}$-Ps-DM1 was nontoxic against human T cells and L929 mouse fibroblasts at DM1 concentrations up to 100 ng/mL, and the viability of L929 cells exceeded 82%, even when the DM1 concentration was increased to 1000 ng/mL (Figures 2f and S4). Furthermore, the free aCD7 nanobody was nontoxic to CCRF-CEM cells at concentrations ranging from 2 to 1000 ng/mL (Figure S5). In the following studies, $aCD7_{5.2}$-Ps-DM1 was used and denoted as aCD7-Ps-DM1.

DM1 reportedly impedes microtubule depolymerization, causes cell cycle arrest, and consequently induces cell apoptosis.[43,44] Therefore, we further analyzed the proapoptotic ability of aCD7-Ps-DM1 and Ps-DM1 using an Annexin V-APC/7-AAD double staining kit. It was found that aCD7-Ps-DM1 induced time-dependent apoptosis of CCRF-CEM cells at a DM1 concentration of 1 ng/mL, with apoptosis rates of 10.2, 18.7, and 29.9% after 4, 12, and 24 h of incubation, respectively (Figure 3). Although nontargeted Ps-DM1 also induced time-dependent cell apoptosis, the percentage of apoptotic cells (5.6−13.0%) was consistently lower than that of aCD7-Ps-DM1-treated cells at all time points.

3.3. In Vivo Anti-T-ALL Effect of aCD7-Ps-DM1 Immuno-Nanotoxin. To study the anti-T-ALL activity of aCD7-Ps-DM1 immuno-nanotoxin in vivo, an orthotopic CCRF-CEM T-ALL model was established by tail vein injection of CCRF-CEM cells into immunodeficient B-NDG mice. On day 5 after cell inoculation, the mice were randomly grouped and administered PBS, Ps-DM1, or aCD7-Ps-DM1 for five injections, with 4 days between each injection (Figure 4a). As shown in Figure 4b−d, CCRF-CEM cells proliferated rapidly in PBS-treated mice, and their proportion in the peripheral blood increased sharply from 25.5 to 51.3% from days 21 to 26, causing sudden weight loss and rapid death, with a median survival of 26 days. Ps-DM1 treatment only slightly slowed T-ALL progression, with 9.5, 24.2, and 37.5% of T-ALL cells in the peripheral blood on days 21, 24, and 27, respectively, and extended the median survival by only 2 days. In contrast, aCD7-Ps-DM1 effectively reduced the

https://doi.org/10.1021/acsanm.3c06253
ACS Appl. Nano Mater. 2024, 7, 7195−7202

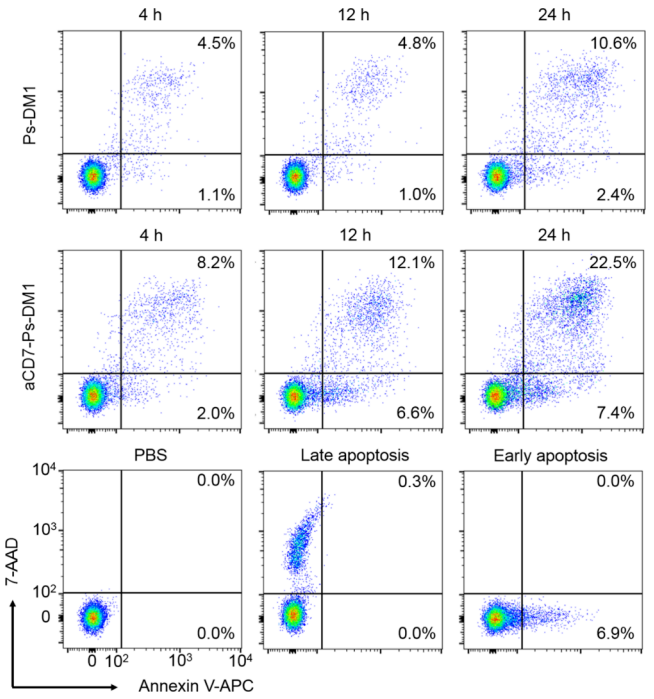

Figure 3. Apoptosis of CCRF-CEM T-ALL cells following 4, 12, or 24 h of incubation with aCD7-Ps-DM1 or Ps-DM1.

burden of CCRF-CEM cells in the peripheral blood to 0.1, 1.4, and 2.3% on days 21−27, which was 22−205- and 16−76-fold lower than that in the PBS and Ps-DM1 groups, respectively (Figure 4b). Accordingly, mouse survival was significantly prolonged (**$p < 0.01$) in comparison to that in the PBS and Ps-DM1 groups (Figure 4c). Of note, both aCD7-Ps-DM1 and Ps-DM1 were well tolerated by mice with no significant weight loss (Figure 4d).

Further evidence was provided by the significant amelioration of hepatosplenomegaly, a common feature of T-ALL patients,[45,46] in aCD7-Ps-DM1-treated mice (Figure 4e). For instance, the weights of spleens from mice treated with aCD7-Ps-DM1 were less than 1/2 compared to those from other control groups. We then analyzed the T-ALL burden in different tissues on day 26 after tumor inoculation using flow cytometry. It was found that CCRF-CEM T-ALL cells severely infiltrated the spleen, liver, and bone marrow of mice in the PBS group, for which the infiltration rate was greater than 85%. The T-ALL burden in the Ps-DM1 group was only marginally reduced, with 77−85.8% infiltration in the spleen, liver, and bone marrow. In sharp contrast, aCD7-Ps-DM1 significantly reduced the T-ALL burden by more than 3.5-fold in various tissues (Figure 4f,g).

Consistent with the flow cytometry-based T-ALL burden analysis, H&E-stained images showed that PBS- and Ps-DM1-treated mice had obvious T-ALL invasion in the liver, spleen, and lung, which was largely inhibited in the aCD7-Ps-DM1 group, showing almost normal histomorphology (Figure 5). No obvious histological destruction was observed in the kidney or heart (Figure S6).

Intensive treatment with eight injections in total was further performed to confirm the anti-T-ALL potential of aCD7-Ps-DM1 (Figure 6a). The results showed that intensive aCD7-Ps-DM1 treatment further inhibited the proliferation of CCRF-CEM T-ALL cells, in which the T-ALL burden in the peripheral blood on day 26 was only 0.2%, not only markedly

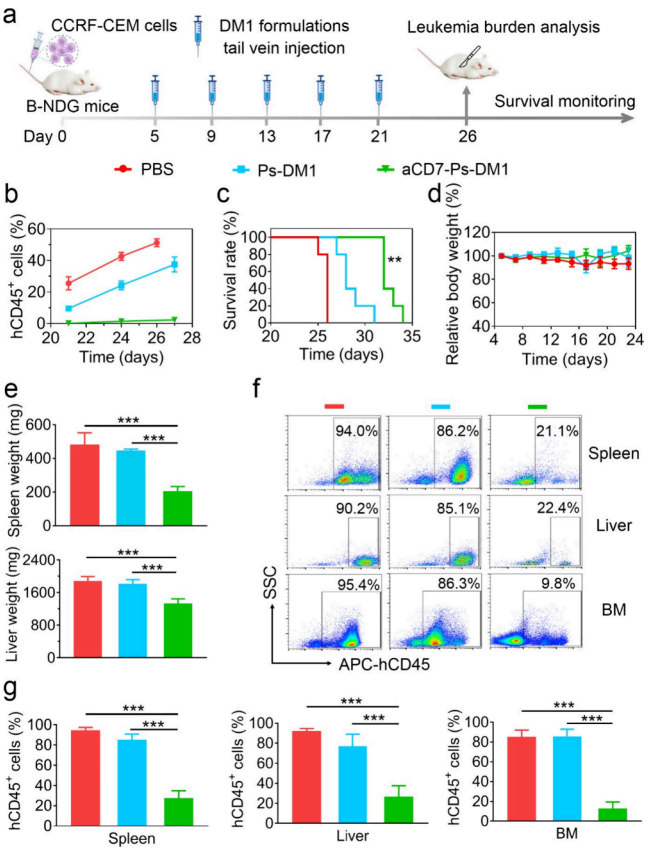

Figure 4. (a) Construction and treatment flowchart of the orthotopic CCRF-CEM T-ALL model. (b) Leukemia burden in the PB, (c) survival curves, and (d) body weight changes of mice ($n = 5$) following different treatments. (e) Weights of spleens and livers isolated from mice in different groups ($n = 4$). (f) Representative scatter diagram and (g) quantitative analysis ($n = 4$) showing the leukemia burden in the spleen, liver, and bone marrow (BM) of mice in different groups on day 26.

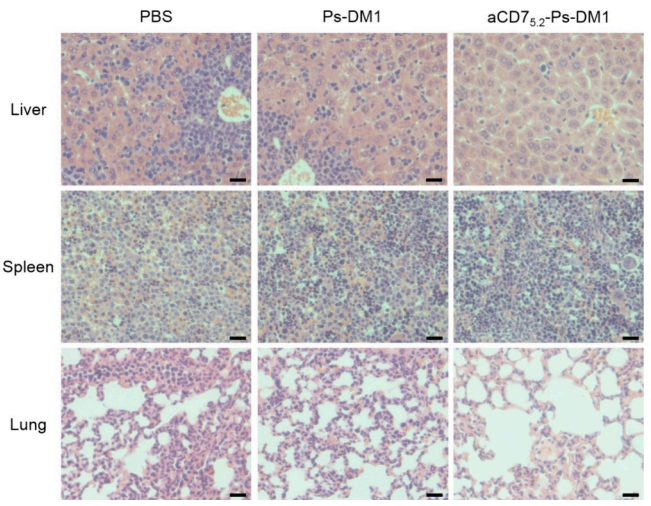

Figure 5. H&E-stained images of liver, spleen, and lung tissues collected from mice in different treatment groups (scale bars: 25 μm).

lower than that in the PBS (53.2%) and Ps-DM1 (14.3%) groups but also lower than that in the five-injection treatment group (2.3%) (Figure 6b). Moreover, CCRF-CEM cells in the peripheral blood of aCD7-Ps-DM1-treated mice, though proliferated over time, remained at a low burden (1.0%)

https://doi.org/10.1021/acsanm.3c06253
ACS Appl. Nano Mater. 2024, 7, 7195−7202

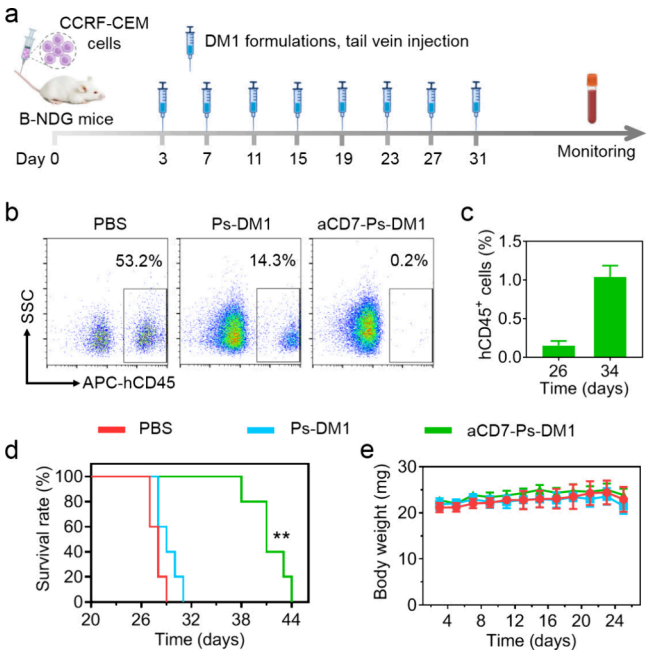

Figure 6. (a) Schematic showing the intensive treatment protocol used for the orthotopic CCRF-CEM-T-ALL model. Leukemia burden in the peripheral blood of (b) PBS-, Ps-DM1-, or aCD7-Ps-DM1-treated mice on day 26 and (c) aCD7-Ps-DM1-treated mice on days 26 and 34 (quantitative analysis, n = 3). (d) Kaplan–Meier survival curves and (e) body weight changes of mice in different treatment groups (n = 5).

even on day 34 post-T-ALL inoculation (Figure 6c). Accordingly, the median survival of mice in the aCD7-Ps-DM1 group was prolonged to 41 days, significantly longer than that of the PBS (27 days) and Ps-DM1 groups (29 days) as well as that of mice receiving five injections of aCD7-Ps-DM1 (32 days) (Figure 6d). Importantly, the intensive administration regimen did not induce obvious side effects or weight loss in mice (Figure 6e).

4. CONCLUSIONS

In summary, a CD7 nanobody-based immuno-nanotoxin is engineered with superb stability and rapid toxin release in an intracellularly mimicking reductive environment, enabling high-efficacy targeted therapy for T-ALL. The immuno-nanotoxin shows high specificity toward CCRF-CEM T-ALL cells and exhibits more than 60-fold greater toxicity than free DM1. Moreover, treating an orthotopic T-ALL model with multiple doses of the CD7-specific immuno-nanotoxin via multiple doses persistently inhibits leukemia progression and significantly prolongs mouse survival. This study reveals that anti-CD7 nanobody-engineered polymersomes are competent for the targeted delivery of DM1 to treat T-ALL, which can be further utilized to deliver molecular targeted agents or first-line chemotherapeutics to offer more effective and safe therapeutic options for T-ALL.

■ ASSOCIATED CONTENT

Supporting Information

The Supporting Information is available free of charge at https://pubs.acs.org/doi/10.1021/acsanm.3c06253.

Details on the characterization and cell culture; size distribution of N_3-P-DM1; HPLC chromatograms of aCD7-Ps-DM1 after incubation with 10 mM GSH; cellular uptake of $aCD7_{5.2}$-Ps-Cy5 and Ps-Cy5 in CD7-negative 697 B-ALL cells; cytotoxicity of aCD7-Ps-DM1 in normal L929 cells and free aCD7 in CCRF-CEM cells; and H&E-stained images of the kidney and heart (PDF)

■ AUTHOR INFORMATION

Corresponding Authors

Huanli Sun − *Biomedical Polymers Laboratory, College of Chemistry, Chemical Engineering and Materials Science, and State Key Laboratory of Radiation Medicine and Protection, Soochow University, Suzhou 215123, P. R. China;* orcid.org/0000-0001-6287-1555; Email: sunhuanli@suda.edu.cn

Lin Yang − *PersonGen BioTherapeutics (Suzhou) Co., Ltd., Suzhou 215123, P. R. China; Cyrus Tang Medical Institute, Collaborative Innovation Center of Hematology, Soochow University, Suzhou 215123, P. R. China*; Email: yanglin@suda.edu.cn

Zhiyuan Zhong − *Biomedical Polymers Laboratory, College of Chemistry, Chemical Engineering and Materials Science, and State Key Laboratory of Radiation Medicine and Protection and College of Pharmaceutical Sciences, Soochow University, Suzhou 215123, P. R. China;* orcid.org/0000-0003-4175-4741; Email: zyzhong@suda.edu.cn

Authors

Yangyang Dong − *Biomedical Polymers Laboratory, College of Chemistry, Chemical Engineering and Materials Science, and State Key Laboratory of Radiation Medicine and Protection, Soochow University, Suzhou 215123, P. R. China*

Fengtao You − *PersonGen BioTherapeutics (Suzhou) Co., Ltd., Suzhou 215123, P. R. China*

Yifan Zhang − *Biomedical Polymers Laboratory, College of Chemistry, Chemical Engineering and Materials Science, and State Key Laboratory of Radiation Medicine and Protection, Soochow University, Suzhou 215123, P. R. China*

Ru Cheng − *Biomedical Polymers Laboratory, College of Chemistry, Chemical Engineering and Materials Science, and State Key Laboratory of Radiation Medicine and Protection, Soochow University, Suzhou 215123, P. R. China;* orcid.org/0000-0002-0879-5069

Songsong Zhao − *Biomedical Polymers Laboratory, College of Chemistry, Chemical Engineering and Materials Science, and State Key Laboratory of Radiation Medicine and Protection, Soochow University, Suzhou 215123, P. R. China*

Complete contact information is available at: https://pubs.acs.org/10.1021/acsanm.3c06253

Author Contributions

The manuscript was written through contributions of all the authors. All the authors have given approval to the final version of the manuscript. Y.D. and F.Y. contributed equally.

Notes

The authors declare no competing financial interest.

■ ACKNOWLEDGMENTS

This work was supported by the National Natural Science Foundation of China (52073196, 52273251, 52073195, and 52233007), the National Key R&D Program of China (2021YFB3800900), and the Natural Science Foundation of

the Jiangsu Higher Education Institutions of China (21KJA150007).

REFERENCES

(1) Belver, L.; Ferrando, A. The genetics and mechanisms of T cell acute lymphoblastic leukaemia. *Nat. Rev. Cancer* **2016**, *16*, 494−507.
(2) Courtois, L.; Cabannes-Hamy, A.; Kim, R.; Delecourt, M.; Pinton, A.; Charbonnier, G.; Feroul, M.; Smith, C.; Tueur, G.; Pivert, C.; Balducci, E.; Simonin, M.; Angel, L. H.; Spicuglia, S.; Boissel, N.; Andrieu, G. P.; Asnafi, V.; Rousselot, P.; Lhermitte, L. IL-7 receptor expression is frequent in T-cell acute lymphoblastic leukemia and predicts sensitivity to JAK inhibition. *Blood* **2023**, *142*, 158−171.
(3) Teachey, D. T.; O'Connor, D. How I treat newly diagnosed T-cell acute lymphoblastic leukemia and T-cell lymphoblastic lymphoma in children. *Blood* **2020**, *135*, 159−166.
(4) Litzow, M. R.; Ferrando, A. A. How I treat T-cell acute lymphoblastic leukemia in adults. *Blood* **2015**, *126*, 833−841.
(5) Malard, F.; Mohty, M. Acute lymphoblastic leukaemia. *Lancet* **2020**, *395*, 1146−1162.
(6) Piya, S.; Yang, Y.; Bhattacharya, S.; Sharma, P.; Ma, H.; Mu, H.; He, H.; Ruvolo, V.; Baran, N.; Davis, R. E.; Jain, A. K.; Konopleava, M.; Kantarjian, H.; Andreeff, M.; You, M. J.; Borthakur, G. Targeting the NOTCH1-MYC-CD44 axis in leukemia-initiating cells in T-ALL. *Leukemia* **2022**, *36*, 1261−1273.
(7) Pocock, R.; Farah, N.; Richardson, S. E.; Mansour, M. R. Current and emerging therapeutic approaches for T-cell acute lymphoblastic leukaemia. *Br. J. Hamaetol.* **2021**, *194*, 28−43.
(8) Zheng, N. S.; Zhao, X. Y.; Wei, D.; Miao, J. L.; Liu, Z. K.; Yong, Y. L.; Zhang, R. Y.; Guo, Y. X.; He, L.; Wang, B.; Sun, X. X.; Yang, H. J.; Zhang, T. J.; He, Q.; Li, X. M.; Zhang, H.; Hou, R.; Lin, P.; Xu, Y. M.; Huang, X. J.; Chen, Z. N.; Bian, H. J. CD147-specific chimeric antigen receptor T cells effectively inhibit T cell acute lymphoblastic leukemia. *Cancer Lett.* **2022**, *542*, No. 215762.
(9) Shimony, S.; DeAngelo, D. J.; Luskin, M. R. Nelarabine: When, where and how to use it when treating T-cell acute lymphoblastic leukemia. *Blood Adv.* **2024**, *8*, 23−26.
(10) Gökbuget, N.; Basara, N.; Baurmann, H.; Beck, J.; Brüggemann, M.; Diedrich, H.; Güldenzoph, B.; Hartung, G.; Horst, H.-A.; Hüttmann, A.; Kobbe, G.; Naumann, R.; Ratei, R.; Reichle, A.; Serve, H.; Stelljes, M.; Viardot, A.; Wattad, M.; Hoelzer, D. High single-drug activity of nelarabine in relapsed T-lymphoblastic leukemia/lymphoma offers curative option with subsequent stem cell transplantation. *Blood* **2011**, *118*, 3504−3511.
(11) Xu, J.; Zhu, H.-H. Targeted treatment of T-cell acute lymphoblastic leukemia: Latest updates from the 2022 ASH annual meeting. *Exp. Hematol. Oncol.* **2023**, *12*, 30.
(12) Abaza, Y.; Kantarjian, M. H.; Faderl, S.; Jabbour, E.; Jain, N.; Thomas, D.; Kadia, T.; Borthakur, G.; Khoury, D. J.; Burger, J.; Wierda, W.; O'Brien, S.; Konopleva, M.; Ferrajoli, A.; Kebriaei, P.; Dabaja, B.; Kornblau, S.; Alvarado, Y.; Daver, N.; Pemmaraju, N.; Bose, P.; Thompson, P.; Al Azzawi, H.; Kelly, M.; Garris, R.; Jain, P.; Garcia-Manero, G.; Cortes, J.; Ravandi, F. Hyper-CVAD plus nelarabine in newly diagnosed adult T-cell acute lymphoblastic leukemia and T-lymphoblastic lymphoma. *Am. J. Hematol.* **2018**, *93*, 91−99.
(13) Brown, P. A.; Shah, B.; Advani, A.; Aoun, P.; Boyer, M. W.; Burke, P. W.; DeAngelo, D. J.; Dinner, S.; Fathi, A. T.; Gauthier, J.; Jain, N.; Kirby, S.; Liedtke, M.; Litzow, M.; Logan, A.; Luger, S.; Maness, L. J.; Massaro, S.; Mattison, R. J.; May, W.; Oluwole, O.; Park, J.; Przespolewski, A.; Rangaraju, S.; Rubnitz, J. E.; Uy, G. L.; Vusirikala, M.; Wieduwilt, M.; Lynn, B.; Berardi, R. A.; Freedman-Cass, D. A.; Campbell, M. Acute lymphoblastic leukemia, version 2.2021, NCCN clinical practice guidelines in oncology. *J. Natl. Compr. Cancer. Network* **2021**, *19*, 1079−1109.
(14) Teachey, D. T.; Hunger, S. P. Immunotherapy for ALL takes the world by storm. *Nat. Rev. Clin. Oncol.* **2018**, *15*, 69−70.
(15) Maciocia, P. M.; Wawrzyniecka, P. A.; Maciocia, N. C.; Burley, A.; Karpanasamy, T.; Devereaux, S.; Hoekx, M.; O'Connor, D.; Leon, T.; Rapoz-D'Silva, T.; Pocock, R.; Rahman, S.; Gritti, G.; Yánez, D. C.; Ross, S.; Crompton, T.; Williams, O.; Lee, L.; Pule, M. A.; Mansour, M. R. Anti-CCR9 chimeric antigen receptor T cells for T-cell acute lymphoblastic leukemia. *Blood* **2022**, *140*, 25−37.
(16) Ren, A.; Tong, X.; Xu, N.; Zhang, T.; Zhou, F.; Zhu, H. CAR T-cell immunotherapy treating T-ALL: Challenges and opportunities. *Vaccines* **2023**, *11*, 165.
(17) You, F. T.; Wang, Y. Y.; Jiang, L. C.; Zhu, X. J.; Chen, D.; Yuan, L.; An, G. L.; Meng, H. M.; Yang, L. A novel CD7 chimeric antigen receptor-modified NK-92MI cell line targeting T-cell acute lymphoblastic leukemia. *Am. J. Cancer Res.* **2019**, *9*, 64−78.
(18) Caracciolo, D.; Mancuso, A.; Polerà, N.; Froio, C.; D'Aquino, G.; Riillo, C.; Tagliaferri, P.; Tassone, P. The emerging scenario of immunotherapy for T-cell acute lymphoblastic leukemia: Advances, challenges and future perspectives. *Exp. Hematol. Oncol.* **2023**, *12*, 5.
(19) Freiwan, A.; Zoine, J. T.; Crawford, J. C.; Vaidya, A.; Schattgen, S. A.; Myers, J. A.; Patil, S. L.; Khanlari, M.; Inaba, H.; Klco, J. M.; Mullighan, C. G.; Krenciute, G.; Chockley, P. J.; Naik, S.; Langfitt, D. M.; Mamonkin, M.; Obeng, E. A.; Thomas, P. G.; Gottschalk, S.; Velasquez, M. P. Engineering naturally occurring CD7− T cells for the immunotherapy of hematological malignancies. *Blood* **2022**, *140*, 2684−2696.
(20) Li, S.; Wang, X.; Yuan, Z.; Liu, L.; Luo, L.; Li, Y.; Wu, K.; Liu, J.; Yang, C.; Li, Z.; Wang, D.; Shen, L.; Ye, X.; He, J.; Han, C.; Wang, Y.; Zhang, D.; Dong, Y.; Fang, L.; Chen, Y.; Sersch, M.; Cao, W. W.; Wang, S. Eradication of T-ALL cells by CD7-targeted universal CAR-T cells and initial test of ruxolitinib-based CRS management. *Clin. Cancer Res.* **2021**, *27*, 1242−1246.
(21) Pan, J.; Tan, Y.; Wang, G.; Deng, B.; Ling, Z.; Song, W.; Seery, S.; Zhang, Y.; Peng, S.; Xu, J.; Duan, J.; Wang, Z.; Yu, X.; Zheng, Q.; Xu, X.; Yuan, Y.; Yan, F.; Tian, Z.; Tang, K.; Zhang, J.; Chang, A. H.; Feng, X. Donor-derived CD7 chimeric antigen receptor T cells for T-cell acute lymphoblastic leukemia: First-in-human, phase I trial. *J. Clin. Oncol.* **2021**, *39*, 3340−3351.
(22) Zhang, M.; Chen, D.; Fu, X.; Meng, H.; Nan, F.; Sun, Z.; Yu, H.; Zhang, L.; Li, L.; Li, X.; Wang, X.; Wang, M.; You, F.; Li, Z.; Chang, Y.; Zhou, Z.; Yan, J.; Li, J.; Wu, X.; Wang, Y.; Wang, Y.; Xiang, S.; Chen, Y.; Pan, G.; Xu, H.; Zhang, B.; Yang, L. Autologous nanobody-derived fratricide-resistant CD7-CAR T-cell therapy for patients with relapsed and refractory T-cell acute lymphoblastic leukemia/lymphoma. *Clin. Cancer Res.* **2022**, *28*, 2830−2843.
(23) Teachey, D. T.; Hunger, S. P. Anti-CD7 CAR T cells for T-ALL: Impressive early-stage efficacy. *Nat. Rev. Clin. Oncol.* **2021**, *18*, 677−678.
(24) Huang, Y.-H.; Wan, C.-L.; Dai, H.-P.; Xue, S.-L. Targeted therapy and immunotherapy for T cell acute lymphoblastic leukemia/lymphoma. *Ann. Hematol.* **2023**, *102*, 2001−2013.
(25) Watanabe, N.; Mo, F.; Zheng, R.; Ma, R.; Bray, V. C.; van Leeuwen, D. G.; Sritabal-Ramirez, J.; Hu, H.; Wang, S.; Mehta, B.; Srinivasan, M.; Scherer, L. D.; Zhang, H.; Thakkar, S. G.; Hill, L. C.; Heslop, H. E.; Cheng, C.; Brenner, M. K.; Mamonkin, M. Feasibility and preclinical efficacy of CD7-unedited CD7 CAR T cells for T cell malignancies. *Mol. Ther.* **2023**, *31*, 24−34.
(26) Fu, Z.; Li, S.; Han, S.; Shi, C.; Zhang, Y. Antibody drug conjugate: The "biological missile" for targeted cancer therapy. *Signal Transduct. Target Ther.* **2022**, *7*, 93.
(27) Dumontet, C.; Reichert, J. M.; Senter, P. D.; Lambert, J. M.; Beck, A. Antibody−drug conjugates come of age in oncology. *Nat. Rev. Drug Discovery* **2023**, *22*, 641−661.
(28) Khongorzul, P.; Ling, C. J.; Khan, F. U.; Ihsan, A. U.; Zhang, J. Antibody−drug conjugates: A comprehensive review. *Mol. Cancer Res.* **2020**, *18*, 3−19.
(29) Tang, J.; Li, J.; Zhu, X.; Yu, Y.; Chen, D.; Yuan, L.; Gu, Z.; Zhang, X.; Qi, L.; Gong, Z.; Jiang, P.; Yu, J.; Meng, H.; An, G.; Zheng, H.; Yang, L. Novel CD7-specific nanobody-based immunotoxins potently enhanced apoptosis of CD7-positive malignant cells. *Oncotarget* **2016**, *7*, 34070−34083.
(30) Wei, J.; Meng, H.; Guo, B.; Zhong, Z.; Meng, F. Organocatalytic ring-opening copolymerization of trimethylene carbonate and dithiolane trimethylene carbonate: Impact of organocatalysts on

https://doi.org/10.1021/acsanm.3c06253
ACS Appl. Nano Mater. 2024, 7, 7195−7202

copolymerization kinetics and copolymer microstructures. *Biomacromolecules* **2018**, *19*, 2294−2301.
(31) Yu, N.; Zhang, Y.; Li, J.; Gu, W.; Yue, S.; Li, B.; Meng, F.; Sun, H.; Haag, R.; Yuan, J.; Zhong, Z. Daratumumab immunopolymersome-enabled safe and CD38-targeted chemotherapy and depletion of multiple myeloma. *Adv. Mater.* **2021**, *33*, No. 2007787.
(32) Gu, W.; An, J.; Meng, H.; Yu, N.; Zhong, Y.; Meng, F.; Xu, Y.; Cornelissen, J. J. L. M.; Zhong, Z. CD44-specific A6 short peptide boosts targetability and anticancer efficacy of polymersomal epirubicin to orthotopic human multiple myeloma. *Adv. Mater.* **2019**, *31*, No. 1904742.
(33) Zhang, Y.; Yue, S.; Haag, R.; Sun, H.; Zhong, Z. An intelligent cell-selective polymersome-DM1 nanotoxin toward triple negative breast cancer. *J. Controlled Release* **2021**, *340*, 331−341.
(34) Zafar, S.; Armaghan, M.; Khan, K.; Hassan, N.; Sharifi-Rad, J.; Habtemariam, S.; Kieliszek, M.; Butnariu, M.; Bagiu, I.-C.; Bagiu, R. V.; Cho, W. C. New insights into the anticancer therapeutic potential of maytansine and its derivatives. *Biomed. Pharmacother.* **2023**, *165*, No. 115039.
(35) Gao, S.; Zhang, W.; Wang, R.; Hopkins, S. P.; Spagnoli, J. C.; Racin, M.; Bai, L.; Li, L.; Jiang, W.; Yang, X.; Lee, C.; Nagata, K.; Howerth, E. W.; Handa, H.; Xie, J.; Ma, Q.; Kumar, A. Nanoparticles encapsulating nitrosylated maytansine to enhance radiation therapy. *ACS Nano* **2020**, *14*, 1468−1481.
(36) Lopus, M.; Oroudjev, E.; Wilson, L.; Wilhelm, S.; Widdison, W.; Chari, R.; Jordan, M. A. Maytansine and cellular metabolites of antibody-maytansinoid conjugates strongly suppress microtubule dynamics by binding to microtubules. *Mol. Cancer Ther.* **2010**, *9*, 2689−2699.
(37) Chen, J.; Jiang, Z.; Zhang, Y. S.; Ding, J.; Chen, X. Smart transformable nanoparticles for enhanced tumor theranostics. *Appl. Phys. Rev.* **2021**, *8*, No. 041321.
(38) Yang, G.; Liu, Y.; Chen, J.; Ding, J.; Chen, X. Self-adaptive nanomaterials for rational drug delivery in cancer therapy. *Acc. Mater. Res.* **2022**, *3*, 1232−1247.
(39) Yuan, Q.; Fan, D.; Zhang, Y.; Yue, S.; Cheng, R.; Zhong, Z.; Sun, H. CD38-selective immuno-nano-DM1 conjugates for depleting multiple myeloma. *Biomater. Sci.* **2023**, *11*, 4985−4994.
(40) Liu, J.; Zhang, Y.; Guo, R.; Zhao, Y.; Sun, R.; Guo, S.; Lu, W.; Zhao, M. Targeted CD7 CAR T-cells for treatment of T-lymphocyte leukemia and lymphoma and acute myeloid leukemia: Recent advances. *Front. Immunol.* **2023**, *14*, No. 1170968.
(41) Tan, Y.; Shan, L. L.; Zhao, L. P.; Deng, B. P.; Ling, Z. J.; Zhang, Y. L.; Peng, S. X.; Xu, J. L.; Duan, J. J.; Wang, Z. L.; Yu, X. J.; Zheng, Q. L.; Xu, X. W.; Tian, Z. L.; Zhang, Y. B.; Zhang, J. C.; Chang, A. H.; Feng, X. M.; Pan, J. Long-term follow-up of donor-derived CD7 CAR T-cell therapy in patients with T-cell acute lymphoblastic leukemia. *J. Hematol. Oncol.* **2023**, *16*, 34.
(42) Zhang, Y.; Li, C.; Du, M.; Jiang, H.; Luo, W.; Tang, L.; Kang, Y.; Xu, J.; Wu, Z.; Wang, X.; Huang, Z.; Zhang, Y.; Wu, D.; Chang, A. H.; Hu, Y.; Mei, H. Allogenic and autologous anti-CD7 CAR-T cell therapies in relapsed or refractory T-cell malignancies. *Blood Cancer J.* **2023**, *13*, 61.
(43) Xu, P.; Wang, R.; Yang, W.; Liu, Y.; He, D.; Ye, Z.; Chen, D.; Ding, Y.; Tu, J.; Shen, Y. A DM1-doped porous gold nanoshell system for NIR accelerated redox-responsive release and triple modal imaging guided photothermal synergistic chemotherapy. *J. Nanobiotechnol.* **2021**, *19*, 77.
(44) Yue, S.; Zhang, Y.; Wei, Y.; Haag, R.; Sun, H.; Zhong, Z. Cetuximab−polymersome−mertansine nanodrug for potent and targeted therapy of EGFR-positive cancers. *Biomacromolecules* **2022**, *23*, 100−111.
(45) Buonamici, S.; Trimarchi, T.; Ruocco, M. G.; Reavie, L.; Cathelin, S.; Mar, B. G.; Klinakis, A.; Lukyanov, Y.; Tseng, J.-C.; Sen, F.; Gehrie, E.; Li, M.; Newcomb, E.; Zavadil, J.; Meruelo, D.; Lipp, M.; Ibrahim, S.; Efstratiadis, A.; Zagzag, D.; Bromberg, J. S.; Dustin, M. L.; Aifantis, I. CCR7 signalling as an essential regulator of CNS infiltration in T-cell leukaemia. *Nature* **2009**, *459*, 1000−1004.
(46) Yang, F.; Feng, W.; Wang, H.; Wang, L.; Liu, X.; Wang, R.; Chen, C.; Yang, X.; Zhang, D.; Ren, Q.; Zheng, G. Monocyte-derived leukemia-associated macrophages facilitate extramedullary distribution of T-cell acute lymphoblastic leukemia cells. *Cancer Res.* **2020**, *80*, 3677−3691.

https://doi.org/10.1021/acsanm.3c06253
ACS Appl. Nano Mater. 2024, 7, 7195−7202